

# Comprehensive and Detailed Kinetic Model of a Traveling Grate Combustor of Biomass

Eliseo Ranzi,<sup>\*,†</sup> Sauro Pierucci,<sup>†</sup> Pier Carlo Aliprandi,<sup>‡</sup> and Silvano Stringa<sup>‡</sup>

<sup>†</sup>Dipartimento di Chimica, Materiali e Ingegneria Chimica “Giulio Natta”, Politecnico di Milano, Piazza Leonardo da Vinci 32, 20133 Milano, Italy

<sup>‡</sup>Garioni Naval SpA, Viale dei Caduti 3, 25030 Castelmella (BS), Italy

**ABSTRACT:** This paper describes a comprehensive model of a biomass combustor on a traveling grate. This general mathematical model deals with the complex multi-phase gas–solid problem of biomass combustion or gasification at both the reactor and particle scale. Mass and energy balances plus proper closure equations describe the behavior of both of the phases. Key elements of the model are the detailed kinetic schemes describing the biomass degradation and the successive gas-phase secondary reactions. The model has been tested and partially validated on a semi-quantitative basis in comparison to a 12 kW biomass combustor operating in Belgium. Model results constitute a useful guideline for control purposes.

## 1. INTRODUCTION

Biomass fuels are a very important energy resource and are gaining an increasingly important role worldwide as a widely diffused, available, and renewable energy source. Besides coal, oil, and natural gas, the fourth largest source of the global primary energy is constituted by biomass that is of key interest mainly in developing countries.<sup>1–3</sup> Biomass combustion for heat and power production on a traveling grate is an interesting and competing technology, because it can fire a wide range of fuels of various dimension and properties (e.g., density, conductivity, heating value, moisture, and ash content). Grate firing is a typical combustion system used for coarse particles of solid fuels. The finer biomass particles are entrained by the flowing primary air and combust in suspension. Pellets and briquettes are the preferential feeds for the fuel bed on the grates. Capacities of grate-fired boilers for burning biomass range from 10 to 40 MW<sub>th</sub>, with the heat release rate per grate area up to 2–4 MW<sub>th</sub>/m<sup>2</sup> as a result of high-volatile and low-ash characteristics of typical biomass fuels.<sup>4,5</sup> In a stationary sloping grate, the grate does not move; the sloping degree is the crucial point of this boiler. The fuel burns as it slides down the slope under gravity. The control of the combustion process is difficult and critical, with the risk of avalanching of the fuel. In the traveling grate, the fuel is fed on one side and is burned while it is transported and controlled by the grate movement. The controlled small layer of the fuel on the grate improves the whole carbon burnout efficiency.

Fluidized-bed combustion and circulating and bubbling fluidized-bed combustion are competing technologies in biomass combustion for heat and power production.<sup>6</sup> Modern grate-firing boilers are one of the combustion technologies suitable or even the preferred technology for biomass combustion for heat and power production.<sup>5,7</sup>

## 2. COMPREHENSIVE MODELING OF THE GRATE COMBUSTOR

Mathematical models of biomass (or coal and solid fuel) gasification and combustion exist at various sophistication levels. For given operating

conditions, a simple mass and energy balance model, together with appropriate thermodynamic and constitutive equations, easily predicts temperatures and fuel gas composition. Since several years,<sup>8</sup> it is well-recognized that a comprehensive and detailed kinetic model of the entire process is required both to determine correctly the biomass conversion and to characterize the location of the maximum temperature or the transient behavior of the fuel bed. In fact, given the biomass composition and the equilibrium temperature, thermodynamic models can simply predict the exit gas composition but they cannot be used for reactor design.<sup>9</sup> There is a need to develop a comprehensive and combined transport and kinetic model, which takes into account the kinetics of homo- and heterogeneous chemical reactions, transport of volatiles produced, and heat and mass transfer between the solid and gaseous phase.<sup>10</sup> Several researchers in recent years<sup>4,5,11–14</sup> have developed reactor models to study biomass conversion in the fuel bed on the grate. A comprehensive model of biomass conversion on the grate needs to approach this multi-phase gas–solid problem at both the reactor and particle scale. Under typical gasification or combustion conditions upon a grate, biomass fuel particles could exhibit relevant internal temperature gradients, which affect the whole decomposition and burning characteristics. At the particle scale, thermally thick particles exhibit significant internal temperature and mass gradients.<sup>13</sup> The Biot number, defined as  $Bi = hd_p/k$  (where  $h$  is the external heat-transfer coefficient,  $k$  is the thermal conductivity, and  $d_p$  is the diameter of the solid particle) is a useful ratio to evaluate the extent of the temperature gradients. Large external heating rates and low thermal conductivity of thick particles create a Biot number >1 and temperature gradients inside the particle. Biomass particles usually have equivalent diameters of 1–10 cm with large Biot numbers ( $Bi = 1–10$ ), under typical combustion conditions. Gradients of temperature, solid fuel composition, and gas concentrations both inside and outside the particles need to be predicted by the model, provided that the proper balance equations and boundary conditions are assumed. External boundary conditions are non-uniform, and three-dimensional (3D) gradients are present inside the particles. To tackle this difficulty, it is expedient to refer to the equivalent spherical diameter of

**Received:** June 21, 2011

**Revised:** July 26, 2011

**Published:** July 28, 2011

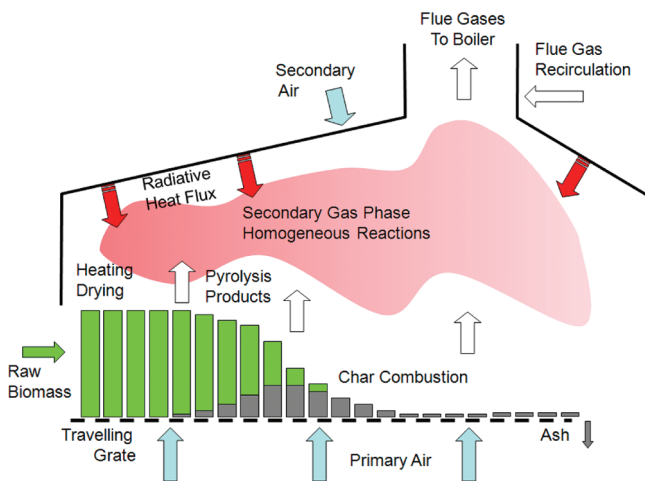


**Figure 1.** Combustor or gasifier unit (from ref 4). Schematic representation of the gas–solid reactor: fixed bed of solid fuel on the grate.

the particles:  $R_p = 6V_p/S_p$ , with  $V_p$  and  $S_p$  being the particle volume and surface, respectively. One-dimensional (1D) spherical coordinates are then used to describe the gradients inside isotropic particles.

A packed bed is formed by many particles resting on each other and supported by a grate. At the reactor scale (Figure 1), the bed on the grate is assumed to be stationary and a vertical stack of several biomass particles, depending upon the bed height, form a slice of the bed. The solution along both the bed height and grate length can be converted into a 1D time-dependent solution, with reference to the traveling speed of the grate.

This approach has been widely used in the literature,<sup>15,16</sup> and this approximation is acceptable for biomass decomposition and combustion on a traveling grate, because of the relatively small horizontal gradients in temperatures and species concentration.<sup>4</sup> The primary air or gas stream fed under the grate flows through the vertical stack of particles. This slice of the moving bed is conveniently simulated through a cascade of ideal reactors, where both the gas phase and solid particles are assumed as well-stirred inside each layer, as shown in Figure 2. Usually, the fuel bed is heated by radiation from the furnace walls and the flames until it devolatilizes, char ignites, and combustion starts at the bed top. The height of the bed shrinks as the flame front travels down toward the grate. The heating, ignition, and propagation of the ignition front in the bed determine the release of volatiles and affect the heat output from the grate.

A comprehensive model of biomass combustion on a grate needs to satisfy several basic requirements, including the necessary condition that the model must conserve the atomic, mass, and energy balances on an integral basis. The model has to describe the combustion front, together with the temperatures, species, and velocity at the top of the fuel bed. This information is used as inlet and closure conditions for the modeling of the secondary gas-phase decomposition and combustion in the freeboard zone. Knowing the flow rates of the biomass fuel, primary and secondary air, and possible flue gas recirculation, the model predicts the profiles of species concentration, temperature, and velocity of the combustion gases leaving the freeboard and entering the boiler. The comprehensive and detailed kinetic model discussed in this work takes into account heat up, drying, pyrolysis, and devolatilization of the fuel particles with char formation, heterogeneous combustion and gasification reactions, and homogeneous gas-phase pyrolysis and oxidation reactions of tar and released species. A multi-step kinetic model describes biomass devolatilization, and a detailed kinetic scheme describes the secondary homogeneous gas-phase reactions. Thus, before the model equations at the particle and reactor scale are discussed, the next section is devoted to present these kinetic models.

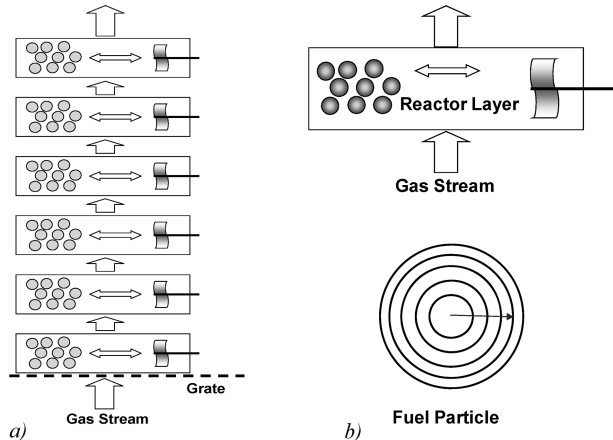


**Figure 2.** Schematic representation of the (a) vertical stack of elementary reactors on the grate and (b) single reactor layer with solid fuel particles.

### 3. KINETIC MODELS

A comprehensive kinetic model, which attempts to tackle the tough, multi-scale, multi-phase problem of biomass conversion in the fuel bed on the grate, needs to analyze heat and mass resistances at both the particle and reactor scale. Apart from the heating and drying of fuel particles, it is necessary to include the following kinetic processes: (3.1) biomass pyrolysis and devolatilization reactions, (3.2) char reactivity, and (3.3) secondary gas-phase reactions and tar conversion.

The next three paragraphs give a brief summary of the main characteristics of the kinetic model, for the biomass devolatilization, the heterogeneous char combustion and gasification reactions, and the successive or secondary gas-phase homogeneous reactions of released species.

**3.1. Biomass Pyrolysis and Devolatilization Reactions.** A simplified, although representative, description of biomass composition is usually given in terms of proximate analysis (moisture, ash, fixed carbon, and volatile matters), elemental analysis (C, H, S, N, and O), or biochemical analysis (cellulose, hemicellulose, and lignin, together with extractives, in either water and ethanol or toluene). The heating value of biomass fuels increases as the lignin content increases. Biomass will be characterized here in terms of the three major components: cellulose, hemicellulose, and lignin, together with inert ashes and moisture. Cellulose is a regular polymer, consisting of a linear chain of glucose units. Hemicellulose is a polysaccharide, derived mainly from glucose and xylose, consisting of shorter and branched chains. Lignin is a more complex polymer with branched and random structures, mainly derived from three monomers: *p*-coumaryl, coniferyl, and sinapyl alcohols.<sup>17</sup> When biochemical analysis is available, it is possible to directly derive biomass composition in terms of cellulose, hemicellulose, lignin, moisture, and ash content. Alternatively, if only elemental analysis in terms of C, H, and O content is accessible, then a suitable combination of the reference species (cellulose, hemicellulose, and lignin) is simply derived from the three atomic balances. Products from biomass pyrolysis are then obtained with a direct combination of the pyrolysis products from the three major components separately. Details on this approach were already reported by Ranzi et al.<sup>18</sup> Hemicellulose breaks down first, at temperatures of 450–550 K. Cellulose follows in the temperature range of 500–620 K, while

**Table 1. Biochar Gasification and Combustion Reactions**  
(Units Are kmol, m<sup>3</sup>, K, and s)<sup>a</sup>

	<i>k</i>
char + O <sub>2</sub> → CO <sub>2</sub>	$1.2 \times 10^{10} \exp(-32300/RT)[\text{char}][\text{O}_2]$
char + 0.5O <sub>2</sub> → CO	$2.5 \times 10^{11} \exp(-38200/RT)[\text{char}][\text{O}_2]^{0.78}$
char + H <sub>2</sub> O → CO + H <sub>2</sub>	$2.5 \times 10^9 \exp(-52000/RT)[\text{char}]^{0.5}[\text{H}_2\text{O}]^{0.70}$

<sup>a</sup> Note that [char] is considered here as the ratio of actual char to the initial char concentration.

lignin components pyrolyze in a wider temperature range of 500–770 K. Cellulose, hemicellulose, and lignin decompose, release gases, and/or form intermediate components that are released and/or involved in substitutive additions and cross-linking reactions with a progressive charification of the solid residue. Levoglucosan (LVG) and hydroxyl-acetaldehyde (HAA) are typical cellulose decomposition products. Xylan is formed by hemicellulose. Phenol and phenoxy species are typical products of lignin decomposition. Typical organic compounds constituting complex bio-oil mixtures are methanol, formic, acetic, and propionic acids, acetone, alcohols, aldehydes, hydroxy-propanone and -butanone, furfural, and methoxy- and dimethoxy-phenols.<sup>19,20</sup>

Table A1 of the Appendix summarizes the full detail of the multi-step devolatilization model, including the reaction heat. Table A2 of the Appendix reports the main volatile species released from biomass devolatilization, together with their formation enthalpy and entropy. The heavy volatile species involved in the kinetic model are lumped species, and they represent a mixture of similar or analogous species with the given average chemical formula. The major features of this devolatilization model, including detailed comparisons with experimental measurements, are reported elsewhere.<sup>18,21</sup>

**3.2. Char Reactivity.** The heterogeneous oxidation and gasification reactions of the residual char are critical for the design of combustion and gasifier units.<sup>22</sup> The rate-determining step is the conversion of the residual char, which influences both the design and the dynamics of the reactors. The gasification and combustion of char, i.e., the set of heterogeneous reactions of oxygen and steam with the solid residue coming from either coal, biomass, or plastics, are responsible for the thermal behavior of the whole process. The residual char formed from biomass pyrolysis is highly reactive, mainly because of its high porosity. The surface area and reactive properties of the char are related to the pyrolysis conditions and the physical and chemical properties of the original biomass. The combustion of volatile matters released by the biomass pyrolysis (flaming combustion) takes place at high temperatures in the freeboard zone, while the burning of active char usually follows the primary volatilization of the fuel particles. Table 1 summarizes the reference kinetic parameters for the combustion and gasification of the biochar obtained from biomass.<sup>23–25</sup> The kinetic parameters of oxidation reactions agree with the ratio CO<sub>2</sub>/CO suggested by Tognotti et al.<sup>26</sup>

**3.3. Secondary Gas-Phase Reactions and Tar Conversion.** Volatile components released by biomasses are subject to successive gas-phase pyrolysis<sup>27</sup> and/or oxidation reactions.<sup>28</sup> The decomposition and combustion of alcohol fuels and other oxygenated species were the subject of recent detailed kinetic studies.<sup>29,30</sup> The complete kinetic model, in CHEMKIN format, together with thermodynamic properties of all involved species, is available on the website.<sup>31</sup> The number of species included in this homogeneous kinetic scheme is a compromise between

accuracy and computational efforts, maintaining the ability of the model to describe the gas composition and reactivity in a wide range of operating conditions; in particular, tar and heavy species are grouped into pseudo-components representative of isomers or analogous species with similar reactivity.

## 4. PARTICLE AND REACTOR MODELS

Basically, the comprehensive model solves energy and mass balance equations for gas and solid phases, together with empirical submodels used for the closure of the balance equations. Devolatilization is a primary process by which the biomass produces residual char, tar, and other heavy species and permanent gaseous products. Released volatiles from biomass particles first mix with the surrounding gas phase in the packed particle bed, only then entering the freeboard zone over the traveling grate. The rate of volatile release depends upon the biomass size and temperature gradient within the particles. The solid fuel bed on the grate is assumed as a stack of several layers. The model presented here considers gas and solid temperature and species profiles not only in the bed but also inside the single particles. Thus, the mathematical model of the whole combustor or gasifier consists of two models: the first one at the particle scale and the latter at the reactor scale. This approach is a further extension of previous models discussed, applied, and validated elsewhere.<sup>23,32,33</sup>

**4.1. Particle Models.** **4.1.1. Thermophysical and Effective Properties of Solid Particles.** Lautenberger and Fernandez-Pello,<sup>34</sup> discussing the mathematical formulation of their Gpyro model for the simulation of combustion and gasification of solid fuels, give a proper emphasis to material property estimations. Usually, the solid fuel is initially composed of several distinct species. Temperature dependencies of thermophysical properties of initial and intermediate solid species are assumed, but combustion and gasification models are not on the whole very sensitive to these temperature dependencies.<sup>22,35</sup> As the particle is heated and pyrolyzed, different gaseous and condensed species are formed. Thermophysical and effective properties of the residual solid particle vary with conversion and are calculated by properly weighting the local compositions.

During the thermal conversion of biomass, also the size and porosity of the individual particles change, not only because of drying and devolatilization but mainly because of char gasification and combustion. Porosity is a property of each condensed phase species and is again calculated as weighted porosity with the local composition. Char porosity significantly varies with the fuel conversion and is estimated on the basis of empirical correlations. These variations are taken into account within the model of the single particles and also within the model of each layer of the entire bed. Therefore, the model accounts for particle and bed shrinkage during biomass conversion.

**4.1.2. Mass and Heat Balances at the Particle Scale.** The particle model provides the internal description to account for intraparticle heat- and mass-transfer resistances, assuming isotropic particles. The accuracy depends upon the number *N* of discretization sectors. This feature becomes fundamental for the analysis of the gasification and combustion of thermally thick solid fuel particles. The heat conduction along the radius of the particle is calculated by solving the heat diffusion equation. Similarly, internal gradients of volatile species are calculated by solving the corresponding continuity equations. Assuming *N* sectors inside the particle, the model equations refer to the mass (solid and gas phase) and energy balances around each particle

sector

$$\left\{ \begin{array}{l} \frac{dm_{j,i}^S}{dt} = V_j R_{j,i} \\ \frac{dm_{j,i}}{dt} = [J_{j-1,i} S_{j-1} - J_{j,i} S_j] + V_j R_{j,i} \\ \frac{d \sum_{i=1}^{NCP} m_{j,i}^S C_{pj,i} T_j}{dt} = [JC_{j-1} S_{j-1} - JC_j S_j] \\ + [S_{j-1} \sum_{i=1}^{NCP} J_{j-1,i} h_{j-1,i} - S_j \sum_{i=1}^{NCP} J_{j,i} h_{j,i}] + V_j HR_j \end{array} \right. \quad (1a)$$

where  $m_{j,i}^S$  is the mass of the  $i$ th solid-phase component,  $m_{j,i}$  is the mass of the  $i$ th volatile component in the  $j$ th particle sector,  $t$  is the time variable, and  $V_j$  and  $S_j$  are the volume and external surface of the  $j$ th particle sector, respectively.  $J$  values are the diffusion fluxes, possibly including also Darcy's contribution. Mass exchange between adjacent sectors is only allowed for volatile species.  $R_{j,i}$  is the net formation rate of the  $i$ th component resulting from the multi-step devolatilization model and from the heterogeneous gas–solid reactions. The energy balance settles the particle temperature  $T$  and accounts for the heat conduction ( $JC$ ), the enthalpy flux relating to the mass diffusion ( $Jh$ ), and the reaction heat (HR). The density profile along the particle radius is calculated as the sum of all of the densities of different species  $m_{j,i}^S$  present in each particle sector. Similarly, the shrinking and porosity of each sector and the whole particle are calculated.

Mass and heat diffusion terms inside the particle follow the constitutive Fick and Fourier laws

$$\left\{ \begin{array}{l} J_{j,i} = -D_{j,i}^{\text{eff}} MW_i \frac{dC_i}{dr} \Big|_{r_j} \\ JC_j = -k_j^{\text{eff}} \frac{dT}{dr} \Big|_{r_j} \end{array} \right. \quad (1b)$$

where  $D_{j,i}^{\text{eff}}$  and  $k_j^{\text{eff}}$  are the effective diffusion and conduction coefficient inside the particle, respectively. At the external surface, these terms are replaced by the flux exchanged with the bulk phase

$$\left\{ \begin{array}{l} J_{N,i} = k_{\text{ext}} MW_i [C_{N,i} - C_i^{\text{bulk}}] \\ JC_N = h_{\text{ext}} [T_N - T^{\text{bulk}}] + JR_N \end{array} \right. \quad (1c)$$

where  $k_{\text{ext}}$  and  $h_{\text{ext}}$  are the mass- and heat-transfer coefficients, respectively, evaluated from the well-known Ranz and Marshall<sup>36</sup> or similar correlations.  $JR_N$  is the net heat transferred by radiation from both the walls and the adjacent solid layers.

**4.2. Reactor Modeling.** The reactor model is practically split into two different parts. First, there is the biomass pyrolysis in the fuel bed on the grate, and then, there are the secondary gas-phase reactions in the freeboard, where special attention has to be paid to the effective mixing to improve combustion and minimize pollutant emissions.

The particle model together with the kinetic models previously described are embedded in the stationary model of the traveling grate reactor. As already mentioned and shown in Figures 1 and 2, the grate movement is converted into a one-dimensional time-dependent solution and the fuel bed on the traveling grate is described by a vertical slice of the bed constituted by a stack of dynamic ideal reactors, where both the gas phase and thick solid

particles are assumed as perfectly stirred. Then, the reactor model requires to describe the freeboard zone, where gas-phase reactions describe the decomposition of the released tar species and the combustion of flue gases.

**4.2.1. Solid Bed.** The whole reactor is considered as a series of  $N_R$  elemental reactors that can exchange mass and heat to each other (Figure 2a). The single unit accounts for gas–solid interactions with particular attention to the interphase resistances, assuming complete mixing for both the gas and solid phase. The height of each bed layer is of the same order of biomass particles, to properly account for vertical dispersion phenomena. It is recognized that the mixing of the main gas flow is further increased because of the energy provided by the volatile species released from the particles during the solid degradation. They increase the turbulence in the system, especially at low air flows through the bed.<sup>37</sup> Furthermore, the movement of the grate promotes a partial vertical mixing of fuel particles.<sup>4,5</sup> The gas-phase mass and energy balance equations refer to the cascade of perfectly stirred reactors in dynamic conditions.

$$\left\{ \begin{array}{l} \frac{dg_i}{dt} = [G_{\text{in},i} - G_{\text{out},i}] + J_{N,i} S_N \eta + V_R R_g, \\ \frac{d \sum_{i=1}^{NCP} g_i C_{pi} T_g}{dt} = [\sum_{i=1}^{NCP} G_{\text{in},i} h_{g_{\text{in},i}} - \sum_{i=1}^{NCP} G_{\text{out},i} h_{g_{\text{out},i}}] \\ + \sum_{i=1}^{NCP} J_{N,i} h_{N,i} S_N \eta + JC_N S_N \eta + V_R HR_g \end{array} \right. \quad (2)$$

As a matter of simplicity, the reactor index (from 1 to  $N_R$ ) is not reported in these balance equations.  $G_{\text{in},i}$  and  $G_{\text{out},i}$  are the inlet and outlet gas streams, respectively, and  $\eta$  is the number of fuel particles in the reactor volume ( $V_R$ ).  $R_g$  stands for the net formation of  $i$  species from the whole secondary gas-phase reactions. The term  $J_{N,i}$  refers to the gas–solid mass exchange and is multiplied by the number of particles in the reactor. Four terms contribute to the evolution of the gas-phase temperature ( $T_g$ ): the enthalpy associated to inlet and outlet streams ( $Gh_g$ ), the gas–solid heat exchange ( $JC_N$ ) and the enthalpy diffusion term ( $J_{N,i} h_{N,i}$ ), both multiplied by the number of particles, and finally, the overall heat contribution because of gas-phase reactions ( $HR_g$ ).

**4.2.2. Freeboard Zone and Gas-Phase Homogeneous Reactions.** Volatile components released by the bed of solid fuel on the grate, together with primary and secondary air or gas streams entering the whole reactor, go through secondary gas-phase decomposition and/or oxidation reactions in the freeboard volume over the solid bed. A proper design and distribution of secondary jets of air or recirculation flue gases ensure the proper mixing in this freeboard zone. Usually, the homogeneous reactions in the burnout zone are not sensitive to the bed pyrolysis and combustion process because of the high-speed flow from secondary jets.<sup>4,38</sup> While the simplest model is constituted by an ideal perfectly stirred reactor, reactor network arrays (RNAs) constitute a simple and feasible option. Dependent upon the complexity of this RNA, the simulation of the freeboard zone could directly move toward more or less complete fluid dynamic computations. The biomass decomposition model describes the release and velocity of volatile species at the top of the fuel bed. This information is used as inlet and closure conditions for the modeling of the secondary gas-phase decomposition of tar and combustion in the freeboard zone. Given the primary and secondary air (and/or different gas streams), the model predicts

the species concentration, temperature, and velocity of the flue gases leaving the freeboard and entering the boiler.

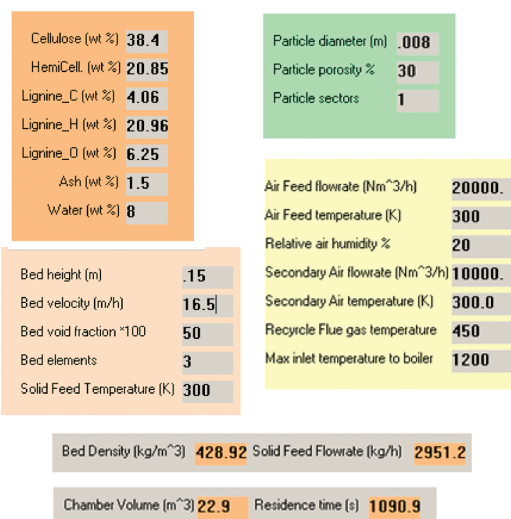
**4.2.3. Radiation Heat Transfer and Closure of the Energy Balance.** As already mentioned, the fuel bed is heated by radiation from both the furnace walls and the flames. Simple radiation heat transfer is considered on the top of the solid fuel bed, and the flue gas temperature is obtained in an iterative way. In fact, to close the whole energy balance on the combustor unit, the gases (burned or oxidized) in the freeboard region need to supply the proper heat to the furnace walls to justify the assumed temperature distribution and the radiation terms in the balance equations.

## 5. NUMERICAL METHODS

The DSMOKE program is used for the gas-phase ideal reactor calculations,<sup>39</sup> while a different code is used for the solution of the multi-phase problem of biomass gasification and combustion. The numerical problem is structured in tridiagonal blocks. The resulting ordinary differential equation (ODE)/differential algebraic equation (DAE) system is solved using the BzzMath Library.<sup>40</sup>



Figure 3. Jets of secondary air in a grate biomass combustor.



More than 1000 balance equations are obtained, when considering ~10–15 solid-phase species, 100 gas-phase components, 8–10 reactor layers, and 5 discretization sectors of the biomass particle. The system of differential equations may present different level of stiffness depending upon the kinetics, the geometries, and the operative conditions. The stiffness degree is the major factor responsible for the computing time, which may vary from a few minutes to some hours. The computing time depends upon the number of equations used to describe the whole process. Experimentally, it has been proven that the computing time versus the problem size varies with a power of ~2.5.

## 6. MODEL PREDICTIONS AND PARAMETRIC SENSITIVITY

**6.1. Model Predictions in Design Operating Conditions.** The model has been tested and partially validated in comparison to experimental data from an industrial biomass combustor designed and installed by Garioni Naval in Belgium. The traveling grate length is approximately 5 m, with less than 3 m of width. The chamber, schematically sketched in Figure 1, has a height varying from 1.2 to 2.0 m, and the flue gas duct width is about 1.7 m. The biomass flow rate is controlled by the grate velocity and the bed height at the entrance of the grate. Primary air crosses the grate and biomass bed from the bottom, while a secondary air is fed through proper devices located on the walls of the chamber. Figure 3 clearly shows not only the position of the combustion front on the grate but also the enhanced gas-phase combustion promoted by the jets of secondary air in the upper part of the freeboard. The flue gas temperature entering the boiler bank is controlled by recirculating flue gas fed at the entrance of the flue gas duct (see Figure 1).

The overall, comprehensive mathematical model described in the previous sections has been implemented in a very flexible code named “GASDS\_GarioniNaval”. Figure 4 summarizes the operating conditions (biomass properties, dimension, flow rate, grate velocity, bed thickness, and primary and secondary air flow rates) together with the overall model predictions. The combustion of 3000 kg/h of biomass with 30 000  $\text{N m}^3 \text{ h}^{-1}$  of primary

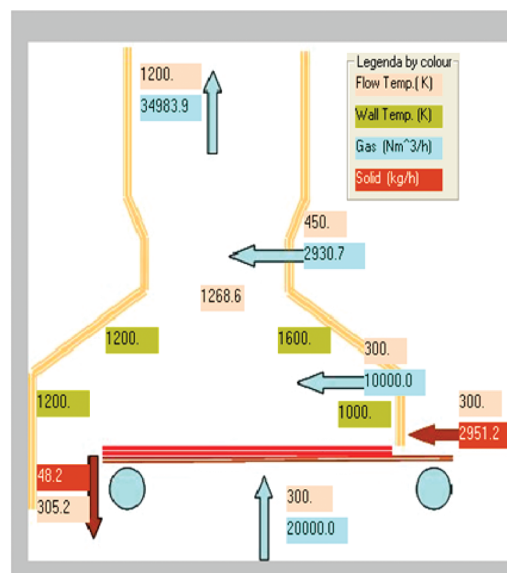
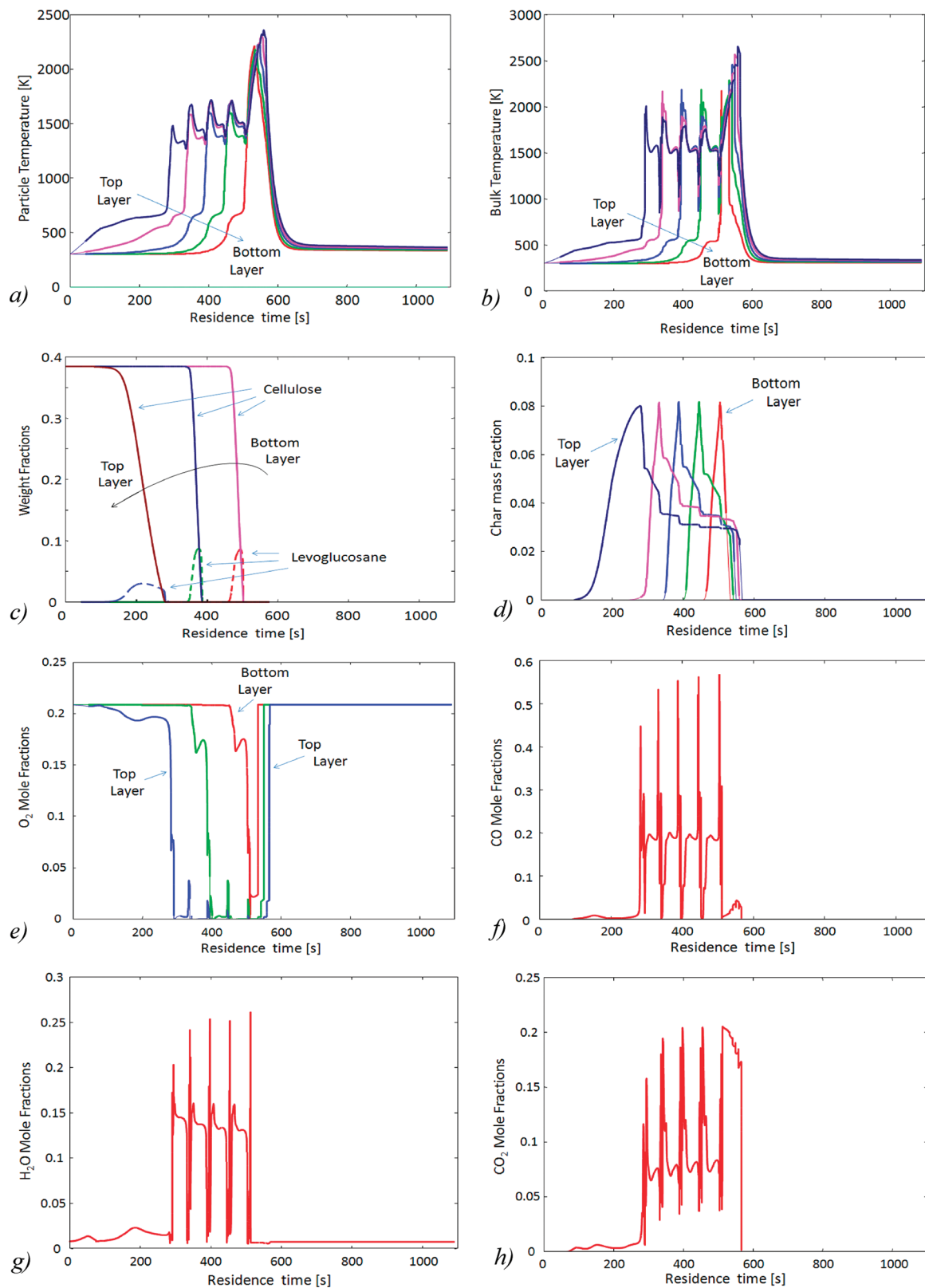


Figure 4. Summary of operating conditions, biomass characteristics, and model predictions.



**Figure 5.** Biomass combustor. Detailed model predictions (five elemental reactor layers): (a and b) particle and gas temperature profiles, (c) cellulose and levoglucosan mass fractions, (d) mass fraction of char in the particle, (e) O<sub>2</sub> mole fraction in the gas stream in the different layers, (f) H<sub>2</sub>O mole fraction released in the freeboard, (g) CO mole fraction released in the freeboard, and (h) CO<sub>2</sub> mole fraction released in the freeboard.

and secondary air gives rise to  $32\ 100\ N\ m^3\ h^{-1}$  of flue gases at  $\sim 1270\ K$ . A stream of  $\sim 35\ 000\ N\ m^3\ h^{-1}$  is fed to the boiler at

the design temperature of  $1200\ K$  by adding  $\sim 2900\ N\ m^3\ h^{-1}$  of recycled exit gases at  $450\ K$ . At a grate speed of  $16.5\ m/h$ , the

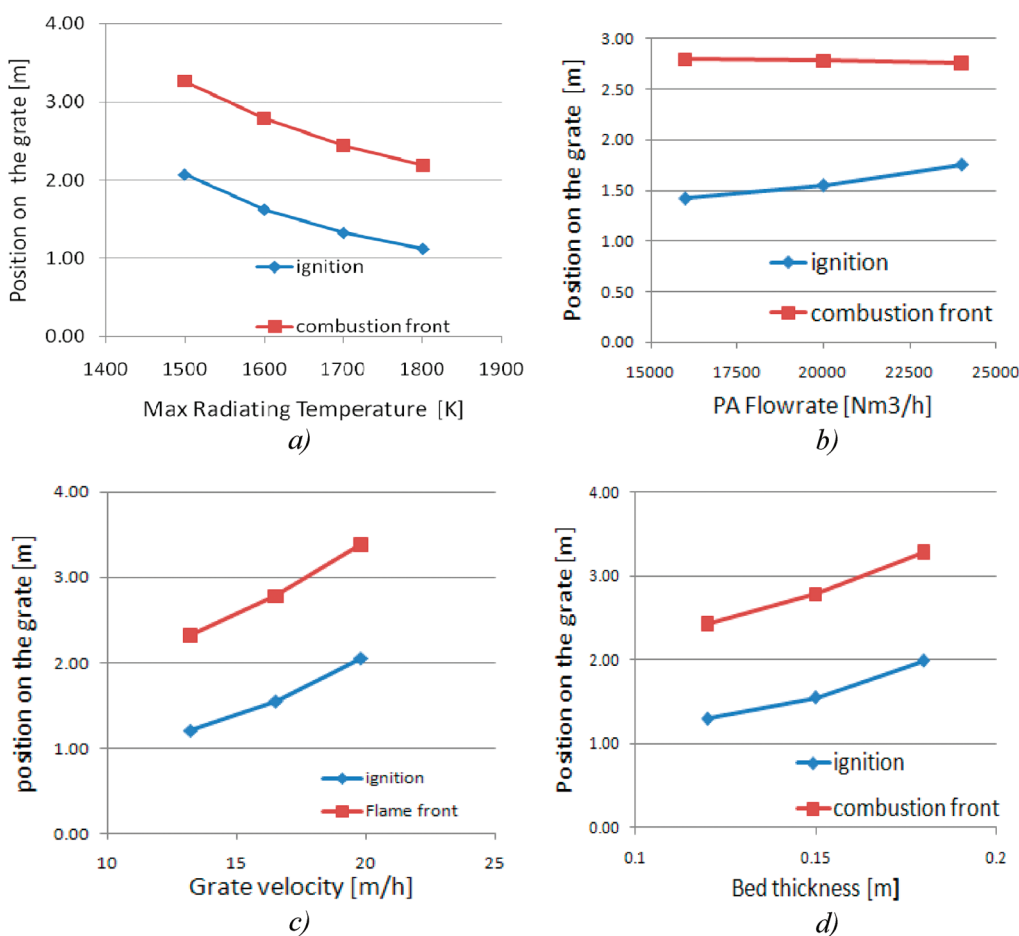


**Figure 6.** Parametric analysis of the mathematical model of the biomass combustor. Position of the combustion front on the grate: (a) effect of the maximum radiating temperature, (b) effect of the primary air flow rate, (c) effect of the grate velocity, and (d) effect of the fuel bed thickness.

residence time on the grate is  $\sim 1100$  s. Figure 5 gives a sample of the detailed information predicted by the model.

The temperature profiles of the gas and solid phase in the fuel bed on the grate clearly indicate that the ignition moves from the top layer, with separate and sudden ignitions of the five different bed layers, with particle temperatures of 1600 K and bulk temperatures even higher than 2000 K. The ignition and combustion front is located in the first half of the traveling grate (at contact times of  $\sim 300$ –600 s). These temperature profiles reflect the layer schematization, and the high peak temperatures are due to both the assumption of small isothermal particles and the lack of the axial thermal diffusion. A larger number of bed layers improves the continuity of temperature profiles, without significant differences in the ignition times, peak temperatures, and overall combustion front. On the contrary, a discretization of the fuel particles reduces the gas peak temperatures, because of a more continuous pyrolysis process with a smoother combustion of released species. Only three or four bed layers, with three sectors to characterize the thick particles, are sufficient to reasonably characterize the combustion behavior of the system. The final oxidation and combustion of char releases a significant reaction heat that is stored in a very modest quantity of residual ash; this is a further reason for the high-temperature peaks, which could be further reduced with a more effective heat exchange with the traveling grate.

The profiles of char formed and oxidized in the different bed layers help the understanding of the overall system. Char is initially

formed in the top layer during the initial heating and pyrolysis. Heating and char formation in the bottom layer occurs only after  $\sim 300$  s. This fact is quite clear when observing the temperature profiles of solid particles and gas stream in the different layers (panels a and b of Figure 5). It is more interesting to observe that char in the top layer remains always present in the combustion front. At high temperatures, oxygen in the primary air is first consumed in the lower bed layers and is not available in the top layers. Thus, char oxidation in the top layer can only be completed at the very end of the combustion process. The effect of the primary air is evident. From one side, primary air maintains moderate temperatures on the grate, and as a consequence, large primary air flow rates delay the ignition of the fuel. From the other side, the primary air flow rate controls the extension of the combustion front, because of the limited O<sub>2</sub> available for char combustion. A large primary air value reduces the width of the combustion front.

These simulations refer to the effective radiant temperature distribution specified in Figure 4. The maximum radiating temperature of  $\sim 1600$  K is strongly related to the distribution of the primary and secondary air and mainly refers to an equivalent flame temperature. The flame temperature over the combustion front depends upon the local combustion stoichiometry, i.e., depends upon primary and secondary air distribution. The flame temperature increases only if a limited fraction of the secondary air is mixed in the freeboard zone directly over the

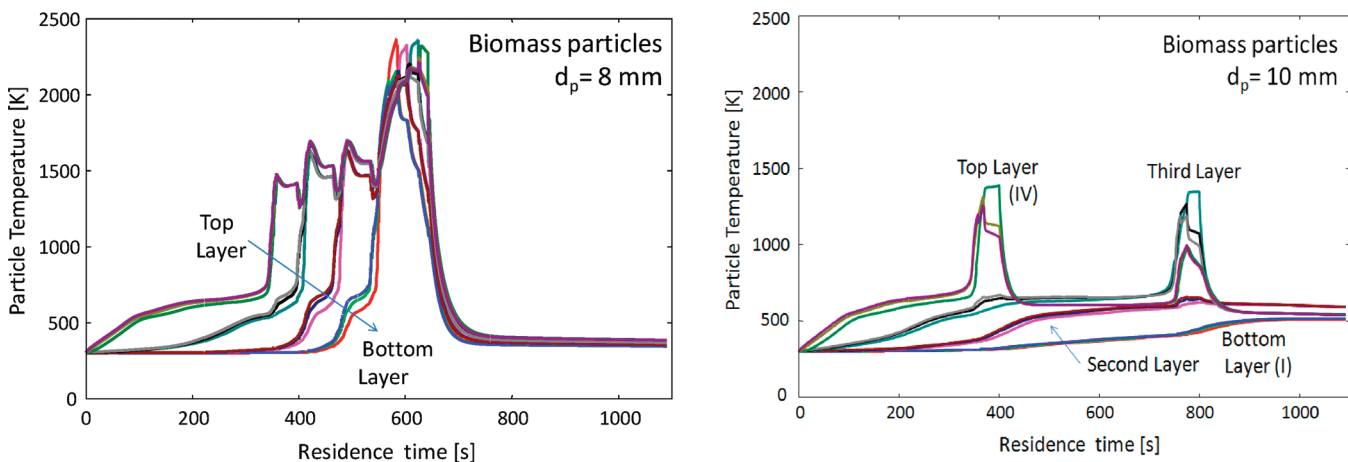


**Figure 7.** Effect of the particle diameter. Predicted temperature profiles of fuel particles of (a) 8 mm and (b) 12 mm.

combustion front. Well-designed jets of secondary air in the postflame zone of the freeboard warrant the proper mixing and combustion completion, just before the bridgewall toward the convective section. Apart from the primary air flow rate, the ignition delay time, i.e., the axial location of the combustion front, mainly depends upon the grate velocity, radiating temperatures, biomass properties, moisture content, etc.

**6.2. Model Sensitivity to Operating Variables.** Model predictions are analyzed here to verify the performance of the grate combustor by varying operating variables and biomass characteristics around the design operating conditions.

**6.2.1. Radiating Temperature.** As already discussed in the previous section, the effective radiating temperature and its distribution is considered as a suitable average value among the temperature of the furnace wall and the temperature of the radiating flame over the grate; then it is a semi-empirical model parameter, which defines the proper distribution of heating rates. The consistency of this distribution is at least partially verified on the basis of the closure of the overall mass and energy balance on the combustor. Figure 6a shows the effect of the radiating temperature on the location of ignition and the end of the combustion front on the grate. While the ignition starts closer to the feed location with the increase of the radiating temperature, the combustion front maintains a constant width on the grate, scarcely dependent upon the radiating temperature. Once the ignition takes place on the fuel bed, then the length of the devolatilization phase, the char formation, and the completion of combustion mainly depend upon oxygen availability in the primary air.

**6.2.2. Primary Air Flow Rates.** Figure 6b shows the effect of the primary air flow rate on the combustion front. Ignition is delayed with the rising of the primary air flow rate, while the width of the combustion front significantly decreases, because of the larger availability of oxygen for the completion of char combustion. A linear correlation exists between char combustion and the primary air flow rate.

**6.2.3. Velocity of the Grate.** The increase of grate velocity has been proposed with a corresponding increase of primary and secondary air flow rates to maintain the combustion stoichiometry, as well as the distribution of primary air and secondary air. Thus, this operating variable corresponds to an increase of the whole capacity of the boiler. As reported in Figure 6c, disregarding boundaries or the bottleneck in the boiler section, the grate combustor is able to treat larger capacities.

**6.2.4. Thickness of the Fuel Bed.** The effect of the thickness of the biomass bed on the grate is reported in Figure 6d, by always maintaining the same grate velocity. Again, the variation of the biomass flow rate is analyzed at fixed combustion stoichiometry; i.e., air flow rates are changed according to the bed thickness. Also, in this case, it is evident that the grate is capable of combusting larger biomass flow rates.

**6.2.5. Particle Diameter.** Panels a and b of Figure 7 show the predicted temperature profiles of fuel particles of 8 and 10 mm, respectively. These simulations refer to a configuration of four reactor layers and three sectors to describe the intraparticle gradients. A first comparison between Figures 5a and 7a shows that, despite the different hypotheses (five or four reactor layers, with or without the thick particle assumption), there is a reasonable convergence in the predicted results, obtained with the same operating conditions. The comparison between panels a and b of Figure 7 shows that the 10 mm particles are not completely burned in these conditions. The first ignition of the top layer takes place at about 340 and 370 s for the 8 and 10 mm particles, respectively. The 10 mm particles, because of their larger sizes and more relevant thermal resistances, are not able to completely devolatilize, and the ignition of the third layer takes place only near to the end of the grate. The fuel particles in the two bottom layers are only heated to ~500–600 K.

The combustion of the biomass particle with diameters larger than 10–12 mm requires more severe conditions and higher heating rates, i.e., higher radiating temperatures in the furnace. The temperature distribution used in the previous examples cannot sustain the complete combustion of large particles. Only the upper layers of the fuel bed on the grate complete the pyrolysis and combustion process, while the core of the particles in the lower reactor layers remains partially unreacted, with a relevant char content in the discharged ash and solid residue.

The model assumes a constant equivalent diameter for all of the fuel particles. The presence of a distribution of particle sizes and the existence of smaller particles contribute to a wider range of complete combustion conditions on the grate. From this viewpoint, model indication and predictions could constitute a safe criterion for the analysis of combustion conditions. On the contrary, the complete combustion of the largest particles in these size distributions also needs to be properly monitored, to avoid incomplete combustion and char content in the ashes.

**Table A1.** Kinetics of Biomass Devolatilization (Units of Kinetic Parameters Are cal, mol, K, and s, and Units of Reaction Heat Are kcal/kg)<sup>a</sup>

reaction	kinetics ( $s^{-1}$ )	heat of reaction
CELL → CELLA	$k = 8 \times 10^{13} \exp(-46000/RT)$	107
CELLA → 0.95HAA + 0.25GLYOX + 0.2CH <sub>3</sub> CHO + 0.25HMFU + 0.2C <sub>3</sub> H <sub>6</sub> O + 0.16CO <sub>2</sub> + 0.23CO + 0.9H <sub>2</sub> O + 0.1CH <sub>4</sub> + 0.61char	$k = 1 \times 10^9 \exp(-30000/RT)$	215
CELLA → LVG	$k = 4T \exp(-10000/RT)$	175
CELL → 5H <sub>2</sub> O + 6char	$k = 8 \times 10^7 \exp(-32000/RT)$	-260
HCE → 0.4HCE1 + 0.6HCE2	$k = 1 \times 10^{10} \exp(-31000/RT)$	131
HCE1 → 0.75G{H <sub>2</sub> } + 0.8CO <sub>2</sub> + 1.4CO + 0.5CH <sub>2</sub> O + 0.25CH <sub>3</sub> OH + 0.125EtOH + 0.125H <sub>2</sub> O + 0.625CH <sub>4</sub> + 0.25C <sub>2</sub> H <sub>4</sub> + 0.675char	$k = 3 \times 10^9 \exp(-27000/RT)$	107
HCE1 → XYLAN	$k = 3T \exp(-11000/RT)$	169
HCE2 → 0.2CO <sub>2</sub> + 0.5CH <sub>4</sub> + 0.25C <sub>2</sub> H <sub>4</sub> + 0.8G{CO <sub>2</sub> } + 0.8G{COH <sub>2</sub> } + 0.7CH <sub>2</sub> O + 0.25CH <sub>3</sub> OH + 0.125EtOH + 0.125H <sub>2</sub> O + char	$k = 1 \times 10^{10} \exp(-33000/RT)$	62
LIG-C → 0.35LIG <sub>CC</sub> + 0.1COUMARYL + 0.08FENOL + 0.41C <sub>2</sub> H <sub>4</sub> + H <sub>2</sub> O + 0.495CH <sub>4</sub> + 0.32CO + G{COH <sub>2</sub> } + 5.735char	$k = 4 \times 10^{15} \exp(-48500/RT)$	144
LIG-H → LIG <sub>OH</sub> + C <sub>3</sub> H <sub>6</sub> O	$k = 2 \times 10^{13} \exp(-37500/RT)$	125
LIG-O → LIG <sub>OH</sub> + CO <sub>2</sub>	$k = 1 \times 10^9 \exp(-25500/RT)$	122
LIG <sub>CC</sub> → 0.3pCOUMARYL + 0.2FENOL + 0.35C <sub>3</sub> H <sub>4</sub> O <sub>2</sub> + 0.7H <sub>2</sub> O + 0.65CH <sub>4</sub> + 0.6C <sub>2</sub> H <sub>4</sub> + G{COH <sub>2</sub> } + 0.8G{CO} + 6.4char	$k = 5 \times 10^6 \exp(-31500/RT)$	69
LIG <sub>OH</sub> → LIG + H <sub>2</sub> O + CH <sub>3</sub> OH + 0.45CH <sub>4</sub> + 0.2C <sub>2</sub> H <sub>4</sub> + 1.4G{CO} + 0.6G{COH <sub>2</sub> } + 0.1G{H <sub>2</sub> } + 4.15char	$k = 3 \times 10^8 \exp(-30000/RT)$	24
LIG → FE2MACR	$k = 8T \exp(-12000/RT)$	138
LIG → H <sub>2</sub> O + 0.5CO + 0.2CH <sub>2</sub> O + 0.4CH <sub>3</sub> OH + 0.2CH <sub>3</sub> CHO + 0.2C <sub>3</sub> H <sub>6</sub> O + 0.6CH <sub>4</sub> + 0.65C <sub>2</sub> H <sub>4</sub> + G{CO} + 0.5G{COH <sub>2</sub> } + 5.5char	$k = 1.2 \times 10^9 \exp(-30000/RT)$	-50

<sup>a</sup> G{H<sub>2</sub>}, G{CO}, and G{COH<sub>2</sub>} are species trapped in the metaplast and successively released to the gas phase.<sup>18</sup>

A similar study of the effect of the kinetic parameters of char reactivity and combustion reactions has shown a limited sensitivity of combustor performances. Similar sensitivity studies on the effect of biomass properties and process parameters on the conversion rate, temperature front, and gas compositions using different bed models are also reported elsewhere.<sup>41–44</sup>

## 7. SUMMARY AND CONCLUSION

A comprehensive mathematical model of biomass combustion on a grate has been presented and validated on the basis of preliminary and semi-quantitative experimental data obtained in an industrial biomass combustor installed by Garioni Naval in Belgium. The freeboard zone is considered here as a simple sequence of well-stirred reactors, and the effect of the optimal

distribution of secondary injection air is not evaluated. Investigations based on complete fluid dynamic analysis of the combustion processes in the freeboard zone are foreseen as future studies, with the aim of controlling CO and volatile organic component (VOC) formation in the flue gas entering the boiler.

Although a mathematical model is in general considered as an effective tool for design purposes, at construction scale, our opinion is that, in the case of biomass combustion, the major benefits of the model are obtained by its capability of predicting trends and sensitivity to operating conditions. The model results reported in this paper clearly show this key feature and the advantage of their use in the control area.

The chemistry applied here to describe the biomass combustion is certainly a detailed one. This is necessarily required by the possibility of the model to cover also the situations in which

**Table A2.** Standard Enthalpy and Entropy of Formation of Main Volatile Species Released from Biomass Devolatilization<sup>18</sup>

chemical name	formula	$\Delta H_f$ (kcal/mol)	$\Delta S_f$ (cal mol <sup>-1</sup> K <sup>-1</sup> )
methanol	CH <sub>4</sub> O	-48.1	57.3
ethanol	C <sub>2</sub> H <sub>6</sub> O	-56.3	67.4
glyoxal	C <sub>2</sub> H <sub>2</sub> O <sub>2</sub>	-50.6	65.42
acetic acid	C <sub>2</sub> H <sub>4</sub> O <sub>2</sub>	-103.9	67.4
hydroxyl-acetaldehyde	C <sub>2</sub> H <sub>4</sub> O <sub>2</sub>	-73.5	73.6
ethylene glicol	C <sub>2</sub> H <sub>6</sub> O <sub>2</sub>	-92.0	76.4
n-propanol	1-C <sub>3</sub> H <sub>7</sub> OH	-60.9	76.4
isopropanol	2-C <sub>3</sub> H <sub>7</sub> OH	-65.1	74.3
hydroxyl-oxo-propanal	C <sub>3</sub> H <sub>4</sub> O <sub>3</sub>	-102.8	88.4
propanal, 3-hydroxy-	C <sub>3</sub> H <sub>6</sub> O <sub>2</sub>	-80.3	83.4
propane-1,3-diol	C <sub>3</sub> H <sub>8</sub> O <sub>2</sub>	-96.9	87.2
propanedial	C <sub>3</sub> H <sub>4</sub> O <sub>2</sub>	-65.8	79.7
n-butanol	C <sub>4</sub> H <sub>10</sub> O	-65.9	85.8
sec-butanol	C <sub>4</sub> H <sub>10</sub> O	-70.0	83.7
isobutanol	C <sub>4</sub> H <sub>10</sub> O	-67.9	83.3
tertbutanol	C <sub>4</sub> H <sub>10</sub> O	-74.5	77.7
furan	C <sub>4</sub> H <sub>4</sub> O	-8.3	63.9
tetrahydrofuran	C <sub>4</sub> H <sub>8</sub> O	-44.2	72.3
butanedione	C <sub>4</sub> H <sub>6</sub> O <sub>2</sub>	-78.4	84.3
xylofuranose	C <sub>5</sub> H <sub>8</sub> O <sub>4</sub>	-151.5	104.9
furan-2-carboxaldehyde	C <sub>5</sub> H <sub>6</sub> O <sub>2</sub>	-36.1	77.8
phenol	C <sub>6</sub> H <sub>6</sub> O	-25.0	76.9
levoglucosan (cellobiosan)	C <sub>6</sub> H <sub>10</sub> O <sub>5</sub>	-200.9	113.7
5-hydroxymethyl-furfural	C <sub>6</sub> H <sub>6</sub> O <sub>3</sub>	-79.8	98.2
2,6-dimethoxy-phenol	C <sub>8</sub> H <sub>10</sub> O <sub>3</sub>	-113.5	134.4

**Table A2. Continued**

chemical name	formula	$\Delta H_f$ (kcal/ mol)	$\Delta S_f$ (cal mol <sup>-1</sup> K <sup>-1</sup> )
4-(3-hydroxy-1-propenyl)-phenol	C <sub>9</sub> H <sub>10</sub> O <sub>2</sub>	-49.8	110.2
3-(4-hydroxy-3,S-dimethoxy-phenyl)-acrylaldehyde	C <sub>11</sub> H <sub>12</sub> O <sub>4</sub>	-116.0	136.8

gasification and combustion phenomena may occur in either sequence or just separately, as in the case of the gasification of biomass, coal, and/or refuse-derived fuels.

## ■ APPENDIX

**Multi-step Kinetic Model of Biomass Pyrolysis.** Kinetics of biomass devolatilization and standard enthalpy and entropy of formation of main volatile species released from biomass devolatilization are provided in Tables A1 and A2, respectively.

## ■ AUTHOR INFORMATION

### Corresponding Author

\*E-mail: eliseo.ranzi@polimi.it.

## ■ ACKNOWLEDGMENT

The authors gratefully acknowledge the useful discussions with Roberto Grana. This research work was partially supported by the Italian Government MSE/CNR (Clean Coal Project).

## ■ NOMENCLATURE

- $C_i$  = gas concentration of component  $i$  (kmol/m<sup>3</sup>)
- $c_{pj,i}$  = heat capacity of component  $i$  in the sector  $j$  (kJ kg<sup>-1</sup> K<sup>-1</sup>)
- $d_p$  = particle diameter (m)
- $D_{ji}^{\text{eff}}$  = effective diffusivity of component  $i$  in the sector  $j$  (m<sup>2</sup>/s)
- $g_i$  = mass of component  $i$  in the gas phase (kg)
- $G_{\text{in},i}$  = inlet gas streams of component  $i$  (kg/s)
- $G_{\text{out},i}$  = outlet gas streams of component  $i$  (kg/s)
- HR = reaction heat (kJ m<sup>-3</sup> s<sup>-1</sup>)
- $h_{\text{ext}}$  = gas–solid heat-transfer coefficient (kJ m<sup>-2</sup> s<sup>-1</sup> K<sup>-1</sup>)
- $h_{ji}$  = specific enthalpy of component  $i$  in the sector  $j$  (kJ/kg)
- $k_j^{\text{eff}}$  = effective thermal conductivity of sector  $j$  (kJ m<sup>-1</sup> K<sup>-1</sup> s<sup>-1</sup>)
- $k_{\text{ext}}$  = gas–solid mass-transfer coefficient (kg/s)
- $J_{ji}$  = mass flux of component  $i$  exiting the sector  $j$  (kg m<sup>-2</sup> s<sup>-1</sup>)
- $J_{\text{C}_j}$  = conductive flux exiting the sector  $j$  (kJ m<sup>-2</sup> s<sup>-1</sup>)
- $J_{\text{R}_N}$  = radiative heat flux at the particle surface (kJ m<sup>-2</sup> s<sup>-1</sup>)
- $m_{ji}^S$  = mass of the  $i$ th solid-phase component in the  $j$ th particle (kg)
- $m_{ji}$  = mass of the  $i$ th volatile component in the  $j$ th particle sector (kg)
- MW = molecular weight (kg/kmol)
- $N$  = number of sectors inside the particle
- $N_R$  = number of reactors in the vertical stack
- $r$  = particle radius (m)
- $R_{g,i}$  = mass production of component  $i$  because of gas-phase reactions (kg m<sup>-3</sup> s<sup>-1</sup>)

$R_{j,i}$  = net formation rate of the  $i$ th component from heterogeneous reactions ( $\text{kg m}^{-3} \text{s}^{-1}$ )  
 $S_j$  = external surface of the  $j$ th particle sector ( $\text{m}^2$ )  
 $t$  = time (s)  
 $T$  = temperature of the solid particle (K)  
 $T_g$  = temperature of the gas phase (K)  
 $V_j$  = volume of the  $j$ th particle sector ( $\text{m}^3$ )  
 $V_p$  = particle volume ( $\text{m}^3$ )  
 $V_R$  = reactor volume ( $\text{m}^3$ )  
 $\eta$  = number of particles in the reactor volume  
 $\varepsilon$  = bed void fraction ( $\text{m}^3/\text{m}^3$ )

## ■ REFERENCES

- (1) McKendry, P. Energy production from biomass (part 3): Gasification technologies. *Bioresour. Technol.* **2002**, *83* (1), 55–63.
- (2) Demirbas, A. Potential applications of renewable energy sources, biomass combustion problems in boiler power systems and combustion related environmental issues. *Prog. Energy Combust. Sci.* **2005**, *31*, 171–192.
- (3) Smeets, E. M. W.; Faaij, A. P. C.; Lewandowski, I. M.; Turkenburg, W. C. A bottom-up assessment and review of global bio-energy potentials to 2050. *Prog. Energy Combust. Sci.* **2007**, *33*, 56–106.
- (4) Yin, C.; Rosendahl, L. A.; Kær, S. K. Grate-firing of biomass for heat and power production. *Prog. Energy Combust. Sci.* **2008**, *34*, 725–754.
- (5) Yin, C.; Rosendahl, L. A.; Kær, S. K.; Clausen, S.; Hvid, S. L.; Hille, T. Mathematical modelling and experimental study of biomass combustion in a thermal 108 MW grate-fired boiler. *Energy Fuels* **2008**, *22*, 1380–1390.
- (6) Gómez-Barea, A.; Leckner, B. Modeling of biomass gasification in fluidized bed. *Prog. Energy Combust. Sci.* **2010**, *36*, 444–509.
- (7) Warnecke, R. Gasification of biomass: Comparison of fixed bed and fluidized bed gasifier. *Biomass Bioenergy* **2000**, *18* (6), 489–497.
- (8) Yoon, H.; Wei, J.; Denn, M. M. A model for moving-bed coal gasification reactors. *AIChE J.* **1978**, *24*, 885–903.
- (9) Di Blasi, C. Dynamic behaviour of the stratified downdraft gasifiers. *Chem. Eng. Sci.* **2000**, *55*, 2931–2944.
- (10) Sheth, P. N.; Babu, B. V. Experimental studies on producer gas generation from wood waste in a downdraft biomass gasifier. *Bioresour. Technol.* **2009**, *100*, 3127–3133.
- (11) Ryu, C.; Shin, D.; Choi, S. Combined simulation of combustion and gas flow in a grate-type incinerator. *J. Air Waste Manage. Assoc.* **2002**, *52*, 174–185.
- (12) Thunman, H.; Leckner, B. Influence of size and density of fuel on combustion in a packed bed. *Proc. Combust. Inst.* **2005**, *30* (2), 2939–2946.
- (13) Yang, Y. B.; Sharifi, V. N.; Swindenbank, J. Numerical simulation of the burning characteristics of thermally-thick biomass fuels in packed beds. *Process Saf. Environ. Prot.* **2005**, *83* (6), 549–558.
- (14) Yang, Y. B.; Newman, R.; Sharifi, V.; Swindenbank, J.; Ariss, J. Mathematical modelling of straw combustion in a 38 MWe power plant furnace and effect of operating conditions. *Fuel* **2007**, *86*, 129–142.
- (15) Shin, D.; Choi, S. The combustion of simulated waste particles in a fixed bed. *Combust. Flame* **2000**, *121*, 167–180.
- (16) Wurzenberger, J. C.; Wallner, S.; Raupenstrauch, H.; Khinast, J. G. Thermal conversion of biomass: Comprehensive reactor and particle modeling. *AIChE J.* **2002**, *48* (10), 2398–2411.
- (17) Klein, M. T.; Virk, P. S. Modeling of lignin thermolysis. *Energy Fuels* **2008**, *22* (4), 2175–2182.
- (18) Ranzi, E.; Cuoci, A.; Faravelli, T.; Frassoldati, A.; Migliavacca, G.; Pierucci, S. Chemical kinetics of biomass pyrolysis. *Energy Fuels* **2008**, *22* (6), 4292–4300.
- (19) Demirbas, A. Progress and recent trends in biofuels. *Prog. Energy Combust. Sci.* **2007**, *33*, 1–18.
- (20) Demirbas, A. Biorefineries: Current activities and future developments. *Energy Convers. Manage.* **2009**, *50*, 2782–2801.
- (21) Calonaci, M.; Grana, R.; Barker Hemings, E.; Bozzano, G.; Dente, M.; Ranzi, E. Comprehensive kinetic modeling study of bio-oil formation from fast pyrolysis of biomass. *Energy Fuels* **2010**, *24* (10), 4265–4273.
- (22) Di Blasi, C. Combustion and gasification rates of lignocellulosic chars. *Prog. Energy Combust. Sci.* **2009**, *35* (2), 121–140.
- (23) Sommariva, S.; Grana, R.; Maffei, T.; Pierucci, S.; Ranzi, E. A kinetic approach to the mathematical model of fixed bed gasifiers. *Comput. Chem. Eng.* **2011**, *35*, 928–935.
- (24) Groeneveld, M. J.; Van Swaaij, W. P. M. Gasification of char particles with  $\text{CO}_2$  and  $\text{H}_2\text{O}$ . *Chem. Eng. Sci.* **1980**, *35*, 307–313.
- (25) Kashiwagi, T.; Nambu, H. Global kinetic constants for thermal oxidative degradation of a cellulosic paper. *Combust. Flame* **1992**, *88* (3–4), 345–368.
- (26) Tognetti, L.; Longwell, J. P.; Sarofim, A. F. The products of the high temperature oxidation of a single char particle in an electrodynamic balance. *Symp. (Int.) Combust., [Proc.]* **1991**, *23* (1), 1207–1213.
- (27) Dente, M.; Pierucci, S.; Ranzi, E.; Bussani, G. New improvements in modelling kinetic schemes for hydrocarbon pyrolysis reactors. *Chem. Eng. Sci.* **1992**, *47*, 2629–2637.
- (28) Ranzi, E. A wide-range kinetic modeling study of oxidation and combustion of transportation fuels and surrogate mixtures. *Energy Fuels* **2006**, *20* (3), 1024–1032.
- (29) Barker-Hemings, E.; Bozzano, G.; Dente, M.; Ranzi, E. Detailed kinetics of the pyrolysis and oxidation of anisole. *Chem. Eng. Trans.* **2011**, *24*, 61–66.
- (30) Grana, R.; Frassoldati, A.; Faravelli, T.; Niemann, U.; Ranzi, E.; Seiser, R.; Cattolica, R.; Seshadri, K. An experimental and kinetic modeling study of combustion of isomers of butanol. *Combust. Flame* **2010**, *157* (11), 2137–2154.
- (31) <http://CRECKModeling.chem.polimi.it/>.
- (32) Pierucci, S.; Ranzi, E. A general mathematical model for a moving bed gasifier. *Comput.-Aided Chem. Eng.* **2008**, *25*, 901–906.
- (33) Dupont, C.; Chen, L.; Cancès, J.; Commandré, J.-M.; Cuoci, A.; Pierucci, S.; Ranzi, E. Biomass pyrolysis: Kinetic modelling and experimental validation under high temperature and flash heating rate conditions. *J. Anal. Appl. Pyrolysis* **2009**, *85* (1–2), 260–267.
- (34) Lautenberger, C.; Fernandez-Pello, C. Generalized pyrolysis model for combustible solids. *Fire Saf. J.* **2009**, *44*, 819–839.
- (35) Recman, M.; Hájek, J. Experimental reactor for analysing biomass combustion properties. *Chem. Eng.* **2009**, *18*, 977–982.
- (36) Ranz, W. E.; Marshall, W. R. Evaporation from drops, part I. *Chem. Eng. Prog.* **1952**, *48*, 141–146.
- (37) Frigerio, S.; Thunman, H.; Leckner, B.; Hermansson, S. Estimation of gas phase mixing in packed beds. *Combust. Flame* **2008**, *153* (1–2), 137–148.
- (38) Klason, T.; Bai, X. S. Computational study of the combustion process and NO formation in a small-scale wood pellet furnace. *Fuel* **2007**, *86*, 1465–1474.
- (39) Manca, D.; Buzzi Ferraris, G.; Faravelli, T.; Ranzi, E. Numerical modeling of oxidation and combustion processes. *Combust. Theory Modell.* **2001**, *5*, 185–199.
- (40) Buzzi Ferraris, G.; Manenti, F. A combination of parallel computing and object-oriented programming to improve optimizer robustness and efficiency. *Comput.-Aided Chem. Eng.* **2010**, *28*, 337–342.
- (41) Yang, Y. B.; Sharifi, V. N.; Swindenbank, J. Effect of air flow rate and fuel moisture on the burning behaviours of biomass and simulated municipal solid wastes in packed beds. *Fuel* **2004**, *83*, 1553–1562.
- (42) Yang, Y. B.; Ryu, C.; Khor, A.; Yates, N. E.; Sharifi, V. N.; Swindenbank, J. Effect of fuel properties on biomass combustion. Part II. Modelling approach—Identification of the controlling factors. *Fuel* **2005**, *84*, 2116–2130.
- (43) Johansson, R.; Thunman, H.; Leckner, B. Sensitivity analysis of a fixed bed combustion model. *Energy Fuels* **2007**, *21*, 1493–1503.
- (44) Zhou, H.; Jensen, A. D.; Glarborg, P.; Jensen, P. A.; Kavaliauskas, A. Numerical modeling of straw combustion in a fixed bed. *Fuel* **2005**, *84*, 389–403.